PCCP

RSC Publishing

PAPER

View Article Online
View Journal | View Issue

Cite this: *Phys. Chem. Chem. Phys.*, 2013, **15**, 1907

Formation and infrared absorption of protonated naphthalenes (1-$C_{10}H_9^+$ and 2-$C_{10}H_9^+$) and their neutral counterparts in solid *para*-hydrogen†

Mohammed Bahou,[a] Yu-Jong Wu*[b] and Yuan-Pern Lee*[ac]

Received 7th September 2012,
Accepted 30th November 2012

DOI: 10.1039/c2cp43143b

www.rsc.org/pccp

Protonated naphthalene ($C_{10}H_9^+$) and its neutral counterparts (hydronaphthyl radicals, $C_{10}H_9$) are important intermediates in the reactions of aromatic compounds and in understanding the unidentified infrared (IR) emissions from interstellar media. We report the IR spectra of 1-$C_{10}H_9^+$, 2-$C_{10}H_9^+$, 1-$C_{10}H_9$, and 2-$C_{10}H_9$ trapped in solid *para*-hydrogen (*p*-H_2); the latter three are new. These species were produced upon electron bombardment of a mixture of naphthalene ($C_{10}H_8$) and *p*-H_2 during matrix deposition. The intensities of IR features of 1-$C_{10}H_9^+$ decreased after the matrix was maintained in darkness for 19 h, whereas those of 1-$C_{10}H_9$ and 2-$C_{10}H_9$ increased. Irradiation of this matrix sample with light at 365 nm diminished lines of 1-$C_{10}H_9^+$ and 2-$C_{10}H_9$ and enhanced lines of 1-$C_{10}H_9$ and 2-$C_{10}H_9^+$; the latter species was unstable and converted to 1-$C_{10}H_9^+$ in less than 30 min and 2-$C_{10}H_9$ was converted to 1-$C_{10}H_9$ at 365 nm. Observed wavenumbers and relative intensities of these species agree satisfactorily with the anharmonic vibrational wavenumbers and IR intensities predicted with the B3PW91/6-311++G(2d,2p) method. Compared with spectra recorded previously with IR photodissociation of Ar-tagged $C_{10}H_9^+$ or IR multiphoton dissociation of $C_{10}H_9^+$, our method has the advantages of producing high-resolution IR spectra with a wide spectral coverage, true IR intensity and excellent ratio of signal to noise; both protonated species and their neutral counterparts are produced with little interference from other fragments. With these advantages, the IR spectra of 1-$C_{10}H_9^+$, 2-$C_{10}H_9^+$, 1-$C_{10}H_9$, and 2-$C_{10}H_9$ are here clearly characterized.

1. Introduction

An enduring mystery in astrochemistry is the source of the 'unidentified infrared (UIR) emission bands' observed from interstellar media (ISM).[1–3] These intense UIR bands consistently observed near 3.3, 6.2, 7.7, 8.6, and 11.3 μm were originally proposed to arise from the infrared (IR) emission of ultraviolet-excited polycyclic aromatic hydrocarbons (PAH),[1,2] because these features correspond to the vibrational bands characteristic of the aromatic C–H and C–C moieties of PAH, but no spectral features of PAH have been found to match exactly the UIR bands.[3,4] Possible candidates of UIR carriers were subsequently extended to include derivatives of PAH, including PAH cations, hydrogenated PAH, dehydrogenated ionic and neutral species, and hetero-nuclear PAH.[1,2,5,6] Among possible forms in this family, protonated PAH (H^+PAH) and its neutral form, mono-hydrogenated PAH (HPAH), have received much attention.[7,8] These species might be formed readily through the protonation of PAH or the attachment of a hydrogen atom to PAH in the ISM.[9–11] In addition, H^+PAH possesses a closed-shell electronic configuration, making the species photochemically stable under the harsh conditions of the astrophysical environment. These species are also known to be intermediates in electrophilic aromatic substitution reactions[12] and in the formation of soot.[13,14]

Naphthalene ($C_{10}H_8$) is the building block of PAH. The spectral investigation of protonated naphthalene ($C_{10}H_9^+$) and its neutral counterparts (hydronaphthyl radicals, $C_{10}H_9$) is fundamental in understanding the UIR emission in ISM.

[a] *Department of Applied Chemistry and Institute of Molecular Science, National Chiao Tung University, 1001, Ta-Hsueh Road, Hsinchu 30010, Taiwan. E-mail: yplee@mail.nctu.edu.tw*
[b] *National Synchrotron Radiation Research Center, 101, Hsin-Ann Road, Hsinchu 30076, Taiwan. E-mail: yjwu@nsrrc.org.tw*
[c] *Institute of Atomic and Molecular Sciences, Academia Sinica, Taipei 10617, Taiwan*

† Electronic supplementary information (ESI) available: Geometric parameters of considered structures of $C_{10}H_9^+$ and $C_{10}H_9$ are summarized in Tables S1–S3 and Tables S4–S6 list predicted vibrational harmonic and anharmonic frequencies of isomers of $C_{10}H_9^+$ and $C_{10}H_9$. See DOI: 10.1039/c2cp43143b

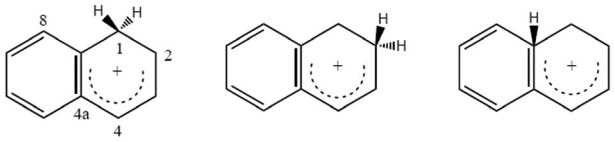

Fig. 1 Structures of isomers of protonated naphthalene: (1) 1-$C_{10}H_9^+$, (2) 2-$C_{10}H_9^+$, and (3) 4a-$C_{10}H_9^+$.

Furthermore, the network of chemical reactions among $C_{10}H_9$, $C_{10}H_9^+$, $C_{10}H_8$, and $C_{10}H_8^+$ has been proposed to occur in the ionosphere of Titan.[15,16] Three distinct protonation sites on naphthalene are possible, as shown in Fig. 1. The most stable structure predicted with theoretical calculations,[17] 1-$C_{10}H_9^+$, has been identified by NMR spectroscopy in solutions of superacid.[18] The electronic spectrum of 1-$C_{10}H_9^+$ was recorded with a band at 19 886 cm^{-1} assigned to the $S_1 \leftarrow S_0$ origin; several resolvable vibronic features were reported.[19,20] Garkusha *et al.* reported electronic absorption spectra of 1-$C_{10}H_9^+$, 2-$C_{10}H_9^+$, 1-$C_{10}H_9$, and 2-$C_{10}H_9$ isolated in solid Ne.[21] Lorenz *et al.* recorded the IR spectrum of gaseous $C_{10}H_9^+$, produced and stored in an ion-cyclotron-resonance ion trap, using IR multiphoton dissociation (IRMPD) with a free-electron laser.[22,23] Ricks *et al.* recorded the IR photodissociation spectrum of the Ar-tagged $C_{10}H_9^+$ complex ($C_{10}H_9^+$-Ar) in the 800–3200 cm^{-1} region.[24] Several features with lines much narrower than those recorded from IRMPD experiments were assigned to 1-$C_{10}H_9^+$-Ar; the spectrum of 1-$C_{10}H_9^+$ is expected to be similar to that of 1-$C_{10}H_9^+$-Ar because the perturbation from Ar is small. Because of the similarity in spectral features, those authors could not positively identify features of 2-$C_{10}H_9^+$-Ar.

The neutralization of $C_{10}H_9^+$ produces the hydronaphthyl radical ($C_{10}H_9$), which is an important intermediate in the reactions of aromatic molecules with hydrogen atoms, especially in combustion systems.[25] Early spectral investigations on hydronaphthyl radicals were limited, with absorption and fluorescence spectra in the visible region,[26,27] EPR spectra,[28,29] and electron-nuclear double-resonance spectra[30] of $C_{10}H_9$ in the naphthalene crystal and in solutions being reported. Vibronic spectra recorded using two-color resonant two-photon ionization (2C-R2PI) of both 1-$C_{10}H_9$ and 2-$C_{10}H_9$ radicals in a supersonic jet were reported in the spectral region 440–530 nm,[31] but all reported vibronic transitions are associated with vibrational modes having wavenumbers less than 500 cm^{-1}. IR spectra enabling identification of $C_{10}H_9$ and distinguishing its various isomers are desirable.

We have employed a 'clean' method to investigate the IR spectra of protonated aromatic hydrocarbons and their neutral counterparts using electron bombardment of *para*-hydrogen (p-H_2) during matrix deposition. We demonstrated the advantages of this method on protonated benzene ($C_6H_7^+$) and cyclohexadienyl radical (c-C_6H_7).[32] Our results clearly indicate that c-C_6H_7 and $C_6H_7^+$ are the only major products; we recorded their IR spectra with much improved resolution, signal-to-noise ratio, and spectral coverage. Furthermore, relative to IR dissociation of Ar-tagged species and IRMPD methods, the IR spectrum of $C_6H_7^+$ reflects the true IR intensity. Our spectrum of c-C_6H_7 provided twice as many lines as those reported for c-C_6H_7 in a Xe matrix.[33] Here, we report an extension from our preceding work on $C_6H_7^+$ and c-C_6H_7 to 1-$C_{10}H_9^+$, 2-$C_{10}H_9^+$, 1-$C_{10}H_9$, and 2-$C_{10}H_9$, which were generated upon electron impact of a gaseous sample of p-H_2 containing a small proportion of naphthalene.

2. Experiments

A gold-plated copper flat cooled to 3.2 K served as a cold substrate for our matrix samples.[34,35] The substrate was cooled using a Janis RDK-415 closed-cycle helium refrigerator system. IR absorption spectra were recorded using a Fourier-transform infrared (FTIR) spectrometer (Bomem, DA8) equipped with a KBr beamsplitter and a Hg–Cd–Te detector (cooled to 77 K), covering the spectral range of 450–5000 cm^{-1}. The copper substrate also served as a mirror to reflect the incident IR beam to the detector. 600 scans at a resolution of 0.25 cm^{-1} were generally recorded at each stage of experiments.

The $C_{10}H_9^+$ cation and $C_{10}H_9$ were produced on electron bombardment of a gaseous sample of p-H_2 containing $C_{10}H_8$ in a small proportion during deposition. An electron gun (Kimball Physics, Model EFG-7) generated electron beams with an energy of 300 eV and a beam current of 70 μA during deposition. Electron bombardment produces H_2^+ that reacts further with H_2 to produce H_3^+ and H. $C_{10}H_9^+$ was produced by proton transfer from H_3^+. Typically, a gaseous mixture of $C_{10}H_8$/p-H_2 (1/1000–1/3000) was deposited over a period of 5–10 h at a flow rate of 13 mmol h^{-1} and the thickness of the matrix was about 0.6–1.0 mm. Photo-irradiation experiments were performed with two light sources. For UV light, a light-emitting diode (Honle UV Technology, 375 mW) with emission at 365 ± 10 nm was used. For visible light, a medium-pressure Hg lamp coupled with a bandpass filter passing 495–700 nm (ESCO Products) was used.

Normal H_2 (99.9999%, Scott Specialty Gases) was passed through a trap at 77 K before entering the p-H_2 converter that comprised a copper cell filled with iron(III) oxide catalyst (Aldrich) and cooled using a closed-cycle refrigerator (Advanced Research Systems, DE204AF). The conversion efficiency was controlled by the temperature of the catalyst; at temperature 11–13 K o-H_2 is less than 100 ppm. Naphthalene (99.8%, Aldrich) vapor at 298 K was mixed with gaseous p-H_2 without further purification.

3. Theoretical calculations

Energies, equilibrium structures, vibrational wavenumbers, and IR intensities were calculated with the Gaussian 09 program.[36] Density-functional theory (DFT) calculations were performed with the B3PW91 method and Becke's three-parameter hybrid exchange functionals,[37] and a Perdew and Wang exchange functional as correlation functional.[38] The standard basis set 6-311++G(2d,2p) was used. Analytic first derivatives were utilized in geometry optimization, and anharmonic vibrational

wavenumbers were calculated analytically at each stationary point. The calculated results including geometric parameters, relative energies, and potential energy profiles are available in ESI† (Tables S1–S3 and Fig. S1–S3). Predicted harmonic and anharmonic vibrational wavenumbers and IR intensities of isomers of $C_{10}H_9^+$ and $C_{10}H_9$ are summarized in Tables S4–S6 (ESI†).

4. Results

A partial IR spectrum of a $C_{10}H_8/p\text{-}H_2$ (1/1500) matrix in the spectral range 700–1650 cm^{-1} is shown in Fig. 2(A). Major lines of $C_{10}H_8$ were observed at 783.8, 959.5, 1012.0, 1137.7, 1210.9, 1268.7, 1392.0, 1513.0, and 1601.5 cm^{-1}, consistent with literature values of 783, 958, 1017, 1141, 1214, 1273, 1392, 1513, and 1602 cm^{-1} for naphthalene isolated in solid Ar,[39,40] and 782, 956, 1012, 1125, 1211, 1268, 1385, 1508, and 1601 cm^{-1} for gaseous naphthalene.[41–46] In the C–H stretching region (not shown), lines of $C_{10}H_8$ were observed at 2971.1, 2988.2, 3011.7, 3027.9, 3041.1, 3062.0, and 3076.2 cm^{-1}, consistent with literature values of 3029.2, 3042.5, 3065.6, and 3078.9 cm^{-1} for naphthalene isolated in solid Ar,[40] and 2980, 2984, 3014, 3025, 3034, 3058, and 3070 cm^{-1} for gaseous naphthalene.[41,44] A partial difference spectrum of the $C_{10}H_8/p\text{-}H_2$ (1/1500) matrix bombarded with an electron beam at 300 eV during deposition for 6 h is shown in Fig. 2(B); to show the new features more clearly, lines of $C_{10}H_8$ were stripped by subtracting the scaled spectrum of $C_{10}H_8$ in $p\text{-}H_2$. These lines form mainly three groups, marked as A, B, and A^+, to be discussed below. Fig. 2(C) depicts a magnified difference spectrum, obtained on subtracting the spectrum of the deposited matrix sample from a spectrum recorded after the matrix was maintained in darkness for 19 h. Lines pointing upward indicate production, whereas those pointing downward indicate destruction. Lines due to absorption of naphthalene are marked as "#" in Fig. 2(C). Because the shape and position of absorption lines of the parent molecules altered slightly over a prolonged period due to self-annealing, the difference spectrum sometimes shows lines with first-derivative shape due to the red or blue spectral shift.

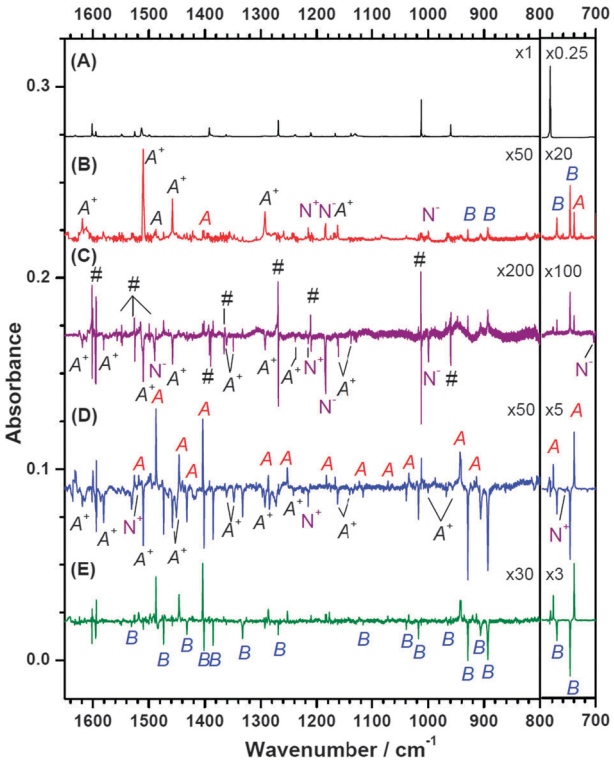

Fig. 2 Partial IR absorption spectra of matrix samples. (A) About 70 mmol of $C_{10}H_8/p\text{-}H_2$ (1/1500) deposited at 3.2 K, (B) electron bombardment of $C_{10}H_8/p\text{-}H_2$ (1/1500, 90 mmol) during deposition at 3.2 K; for clarity of showing the products, lines due to $C_{10}H_8$ are stripped and only the intense lines are marked, (C) difference spectrum of the electron-bombarded matrix sample, prepared in a separate experiment, after maintaining in darkness for 19 h; features indicated with A^+ are due to 1-$C_{10}H_9^+$; those with # are due to interference from bands of $C_{10}H_8$, and lines indicated with N^+ are due to absorption of $C_{10}H_8^+$, and N^- are due to $C_{10}H_8^-$, (D) difference spectrum of the sample in (B) upon irradiation at 365 nm for 2.5 h; features indicated with A are due to 1-$C_{10}H_9$, (E) the spectrum in (D) with lines in group A^+ stripped to show clearly lines in group B, assigned to 2-$C_{10}H_9$. Zooming factors are indicated for each trace.

Downward lines in a set with intense ones at 1618.7, 1580.8, 1510.0, 1457.9, 1361.2, 1292.4 and 1162.7 cm^{-1} are likely associated with an ionic species because of its slow reaction with electrons in $p\text{-}H_2$. These lines, showing a correlated variation of intensity over various experimental steps, are designated as group A^+ in Fig. 2(C) and assigned to 1-$C_{10}H_9^+$, to be discussed in Section 5.1. A list of observed lines in group A^+ is given in Table 1. Because of the small ionization energy (8.14 eV)[47] and small negative electron affinity (−0.20 eV)[48,49] of naphthalene, both cationic and anionic naphthalene might be produced during electron impact of the matrix sample. The extremely weak downward lines at 1215.4, 1525.1 and 756.0 cm^{-1} (indicated with N^+ in Fig. 2C and D) are similar to three most intense lines at 1218.0, 1525.7 and 758.7 cm^{-1} assigned to the naphthalene cation ($C_{10}H_8^+$) in solid Ar,[39] so we assigned them to $C_{10}H_8^+$ in solid $p\text{-}H_2$ with an estimated concentration less than 1 ppm. Another set of downward lines at 703.5, 999.3, 1183.9, and 1489.8 cm^{-1} (indicated with N^- in Fig. 2C) is assigned to $C_{10}H_8^-$ because their positions and relative intensities are similar to those reported for $C_{10}H_8^-$ in a tetrahydrofuran solution at 77 K;[50] the estimated concentration was less than 3 ppm. The upward lines are expected to be due to neutral species and are grouped into A and B, but they are relatively weak. We discuss these features in the results of photo-irradiation experiments as they became more enhanced after these experiments.

To distinguish further the spectral features of neutral species, we irradiated the deposited samples at various wavelengths to identify lines in various groups according to their correlations in intensity in each experiment. A difference spectrum following photolysis at 365 nm for 2.5 h using a light-emitting diode is shown in Fig. 2(D); irradiation of the matrix with UV light not only released electrons trapped in the matrix but might also photodissociate or photoisomerize neutral or ionic aromatic species. As shown in Fig. 2(D), the intensity of features in group A^+ decreased upon UV photolysis. In addition, a second set of

Table 1 Comparison of experimental and theoretical vibrational wavenumbers (in cm^{-1}) and relative IR intensities of 1- and 2-$C_{10}H_9^+$

		1-$C_{10}H_9^+$		2-$C_{10}H_9^+$		
Mode	Sym	Prediction[a]	p-H_2[b]	Prediction[a]	p-H_2[b]	IRPD $C_{10}H_9^+$-Ar[c]
ν_1	A′	3102 (0)		3097 (0)		3082
ν_2	A′	3087 (1)		3086 (0)		
ν_3	A′	3090 (0)		3095 (0)		
ν_4	A′	3079 (0)		3084 (0)		
ν_5	A′	3076 (1)		3076 (1)		
ν_6	A′	3049 (0)		3065 (0)		
ν_7	A′	3032 (0)		3072 (0)		
ν_8	A′	2850 (13)	2844.7 (11?)	2841 (26)	2829.4 (40)	2850
ν_9	A′	1625 (37)	1618.7 (40)	1627 (100)	1623.9 (100)	1617
ν_{10}	A′	1571 (27)	1580.8 (21)	1610 (11)	1602.9 (5?)	1575
ν_{11}	A′	1558 (5)	1556.7 (7)	1563 (2)		
ν_{12}	A′	1515 (100)	1510.0 (100)	1507 (13)	1505.4 (7?)	1506
ν_{13}	A′	1458 (54)	1457.9 (70)	1471 (49)	1472.0 (25)	1480
ν_{14}	A′	1449 (1)		1440 (1)		1454
ν_{15}	A′	1420 (13)	1421.7 (14)	1405 (4)		1418
ν_{16}	A′	1365 (34)	1361.2 (34)	1402 (42)	1399.1 (31)	1391/1378
ν_{17}	A′	1346 (8)	1347.6 (8)	1335 (13)	1336.6 (4)	1358
ν_{18}	A′	1286 (46)	1292.4 (50)	1289 (22)	(ov-1-H^+ N)[d]	1295
ν_{19}	A′	1278 (9)	1274.8 (9)	1268 (56)	1265.6 (60)	1271/1252
ν_{20}	A′	1252 (10)	1242.1 (5)	1249 (2)		1236
ν_{21}	A′	1201 (3)	1199.0 (2)	1218 (2)		
ν_{22}	A′	1182 (4)	1175.0 (6)	1185 (7)	1177.8? (12)	
ν_{23}	A′	1170 (13)	1162.7 (23)	1167 (9)	1156.8 (10)	1164
ν_{24}	A′	1141 (3)	1132.0? (2)	1148 (2)		
ν_{25}	A′	1099 (4)	1094.3 (4)	1025 (7)	1034.3? (10)	1095
ν_{26}	A′	1037 (1)		1025 (1)		
ν_{27}	A′	963 (6)	956.0 (5)	930 (2)		958
ν_{28}	A′	920 (0)		926 (9)	920.5 (12)	
ν_{29}	A′	791 (0)		778 (2)		
ν_{30}	A′	745 (2)		745 (2)		
ν_{31}	A′	603 (1)		609 (1)		
ν_{32}	A′	496 (4)		502 (0)		
ν_{33}	A′	497 (3)		496 (2)		
ν_{34}	A′	352 (0)		358 (1)		
ν_{35}	A″	2844 (4)	2839.1 (3?)	2824 (6)	2819.3 (8)	
ν_{36}	A″	1138 (0)		1120 (0)		
ν_{37}	A″	1018 (0)		1019 (0)		
ν_{38}	A″	1016 (0)		1001 (0)		
ν_{39}	A″	1000 (2)	996.5 (4)	992 (1)		
ν_{40}	A″	977 (0)		937 (7)	935.3 (8)	
ν_{41}	A″	904 (0)		891 (4)		
ν_{42}	A″	840 (3)	841.8 (4)	796 (7)	799.2 (11)	
ν_{43}	A″	773 (23)	772.0 (35?)	778 (0)		
ν_{44}	A″	726 (12)	727.0 (12)	768 (19)	767.7 (15)	
ν_{45}	A″	653 (0)		653 (1)		
ν_{46}	A″	472 (0)		471 (9)		
ν_{47}	A″	423 (5)		434 (2)		
ν_{48}	A″	393 (0)		365 (1)		
ν_{49}	A″	245 (5)		264 (1)		
ν_{50}	A″	169 (1)		163 (0)		
ν_{51}	A″	119 (0)		135 (2)		

[a] Anharmonic vibrational wavenumbers of 1- and 2-$C_{10}H_9^+$ were calculated with the B3PW91/6-311++G(2d,2p) method. Relative intensities listed in parentheses were normalized to the most intense line of ν_{12} of 1-$C_{10}H_9^+$ and ν_9 of 2-$C_{10}H_9^+$ that were calculated to be 230.5 and 236.1 km mol^{-1}, respectively. [b] Mark "?" denotes tentative assignments or uncertain values due to interference with other lines. [c] IRPD (infrared photodissociation) data of $C_{10}H_9^+$-Ar are taken from ref. 24. [d] Overlapped with 1-$C_{10}H_9^+$.

downward-pointing features was observed with intense and moderately intense lines at 1473.4, 1432.2, 1401.3, 1385.1, 1332.6, 1269.0, 1017.0, 928.7, 906.1, 893.1, 771.4, and 747.1 cm^{-1} (group B). To illustrate the downward lines of group B more clearly, we stripped the downward lines of group A^+ in Fig. 2(D) and present the resulting spectrum in Fig. 2(E). These features designated as group B in Fig. 2(E) are assigned to 2-$C_{10}H_9$, to be discussed in Section 5.2. The upward-pointing features with intense and moderately intense lines at 1487.3, 1446.0, 1403.9, 942.3, 778.1, 739.8, and 648.5 cm^{-1} are designated as group A and assigned to 1-$C_{10}H_9$, to be discussed in Section 5.2. Lists of observed lines of 1-$C_{10}H_9$ and 2-$C_{10}H_9$ are given in Table 2.

In the CH-stretching region, the grouping is less certain; some lines might be missing because of the congestion of lines and interference from lines of the parent or other products. From comparison of the difference spectra of the matrix

Table 2 Comparison of experimental and theoretical vibrational wavenumbers and relative IR intensities of 1- and 2-$C_{10}H_9$

		1-$C_{10}H_9$		2-$C_{10}H_9$	
Mode	Sym.	Prediction[a]	p-H_2[b]	Prediction[a]	p-H_2[b]
ν_1	A′	3054 (25)	3051.9? (13?)	3069 (22)	3080.7 (22?)
ν_2	A′	3074 (41)	3073.0 (38?)	3062 (30)	3063.9 (30)
ν_3	A′	3061 (48)	3057.4 (28)	3048 (30)	3045.3 (10?)
ν_4	A′	3067 (12)		3050 (10)	3042.4 (10?)
ν_5	A′	3048 (2)		3047 (14)	3023.5 (6)
ν_6	A′	3023 (16)	3015.3 (12?)	3043 (6)	
ν_7	A′	3048 (7)	3048.2? (1)	2988 (4)	2996.4 (2)
ν_8	A′	2865 (47)	2843.5 (20?)	2844 (67)	2795.8 (9?)
ν_9	A′	1597 (1)		1639 (0)	
ν_{10}	A′	1555 (0)		1564 (0)	
ν_{11}	A′	1523 (4)	1518.3 (3)	1533 (3)	1531.2 (1)
ν_{12}	A′	1488 (14)	1487.3 (13)	1475 (7)	1473.4 (7)
ν_{13}	A′	1448 (12)	1446.0 (10)	1434 (5)	1432.2 (4)
ν_{14}	A′	1410 (0)		1420 (5)	1418.2 (3?)
ν_{15}	A′	1409 (19)	1403.9 (17)	1407 (8)	1401.3 (6)
ν_{16}	A′	1363 (1)	1364.2 (1)	1386 (4)	1385.1 (5)
ν_{17}	A′	1337 (0)	1325.7 (1)	1327 (7)	1332.6 (5)
ν_{18}	A′	1294 (9)	1286.5 (6)	1326 (0)	
ν_{19}	A′	1255 (6)	1252.5 (4)	1274 (6)	1269.0 (2?)
ν_{20}	A′	1213 (1)		1225 (1)	
ν_{21}	A′	1182 (3)	1182.7 (2)	1184 (0)	
ν_{22}	A′	1163 (0)		1161 (1)	1139.8 (1)
ν_{23}	A′	1157 (0)		1147 (1)	1137.4 (1)
ν_{24}	A′	1127 (4)	1122.6 (2)	1121 (3)	1116.2 (2)
ν_{25}	A′	1079 (4)	1071.6 (2)	1040 (4)	1038.8 (2)
ν_{26}	A′	1042 (6)	1034.1 (2)	1024 (6)	1017.0 (4)
ν_{27}	A′	945 (19)	942.3 (20)	910 (1)	
ν_{28}	A′	913 (1)	913.4 (2)	894 (22)	893.1 (20)
ν_{29}	A′	784 (2)		771 (1)	
ν_{30}	A′	743 (0)		744 (0)	
ν_{31}	A′	603 (1)		604 (2)	600.1 (3)
ν_{32}	A′	497 (1)		498 (0)	
ν_{33}	A′	480 (1)		483 (1)	
ν_{34}	A′	354 (1)		353 (1)	
ν_{35}	A″	2817 (18)	2787.1 (13?)	2773 (18)	2779.2 (10?)
ν_{36}	A″	1173 (1)	1177.1 (1)	1154 (0)	
ν_{37}	A″	982 (0)		974 (1)	964.6 (1)
ν_{38}	A″	951 (0)		970 (0)	
ν_{39}	A″	946 (4)		937 (9)	928.7 (10)
ν_{40}	A″	915 (3)	913.4 (3)	904 (11)	906.1 (9)
ν_{41}	A″	857 (1)		854 (0)	
ν_{42}	A″	781 (35)	778.1 (41)	773 (23)	771.4 (31)
ν_{43}	A″	742 (100)	739.8 (100)	749 (100)	747.1 (100)
ν_{44}	A″	700 (15)	696.1 (12)	686 (1)	
ν_{45}	A″	649 (51)	648.5 (51)	673 (1)	674.6 (3)
ν_{46}	A″	533 (2)	527.4 (3)	530 (8)	528.5 (4)
ν_{47}	A″	464 (4)		448 (24)	
ν_{48}	A″	420 (14)		385 (0)	
ν_{49}	A″	249 (11)		247 (0)	
ν_{50}	A″	167 (1)		166 (3)	
ν_{51}	A″	92 (0)		121 (2)	
Combination and overtone bands			1797.7 (2)		2649.7 (4)
			1821.8 (2)		2746.0 (7)
			1877.2 (2)		2767.1 (3)
			2826.8 (5?)		2771.6 (1)
			2833.8 (15?)		2791.7 (8?)
			2847.5 (4?)		2820.1 (10?)
			2854.5 (8)		

[a] Anharmonic vibrational wavenumbers of 1- and 2-$C_{10}H_9$ were calculated with the B3PW91/6-311++G(2d,2p) method. Relative intensities listed in parentheses were normalized to the most intense line of ν_{43} of 1-$C_{10}H_9$ and 2-$C_{10}H_9$ that were calculated to be 56.4 and 74.8 km mol^{-1}, respectively. [b] Mark "?" denotes tentative assignments or uncertain values due to interference with other lines.

irradiated with UV light and stored in darkness for a protracted period, the weak lines at 2844.7 and 2839.1 cm^{-1}, invariably pointing downward in the both cases, are readily assigned to group A^+. Similarly, lines at 3073.0, 3057.4, 2843.5, and 2787.1 cm^{-1}, pointing upward in both cases and with moderate intensity, are assigned to group A, whereas lines at 3080.7,

3063.9, 3023.5, 2795.8, and 2779.2 cm^{-1}, showing an opposite trend in the two cases and with moderate intensity, are assigned to group B.

We attribute most new features in Fig. 2(B) to groups A^+ ($1\text{-}C_{10}H_9^+$), A ($1\text{-}C_{10}H_9$), and B ($2\text{-}C_{10}H_9$). When we employed the theoretically predicted IR intensities and compared the observed integrated intensities of representative intense lines in each group, we estimated the relative mixing ratios to be approximately $[1\text{-}C_{10}H_9^+] : [1\text{-}C_{10}H_9] : [2\text{-}C_{10}H_9] : [C_{10}H_8] = 1.0 : 1.9 : 3.4 : 29$, after deposition (Fig. 2B); the concentration of $C_{10}H_8$ was ~540 ppm. The most intense line of $1\text{-}C_{10}H_9^+$ at 1510.0 cm^{-1} has an IR intensity of 231 km mol^{-1}, whereas those of $1\text{-}C_{10}H_9$ at 739.8 cm^{-1} and of $2\text{-}C_{10}H_9$ at 747.1 cm^{-1} have IR intensities of 56 and 75 km mol^{-1}, respectively. Hence, at the same mixing ratios, the line of $1\text{-}C_{10}H_9^+$ at 1510.0 cm^{-1} appears to be more intense than those near 740 cm^{-1} for $1\text{-}C_{10}H_9$ and $2\text{-}C_{10}H_9$. In a separate experiment, $[1\text{-}C_{10}H_9^+] : [1\text{-}C_{10}H_9] : [2\text{-}C_{10}H_9] : [C_{10}H_8] = 1.0 : 3.2 : 6.4 : 35$ and $[C_{10}H_8] \cong 540$ ppm after deposition. After 19 h, the variations in mixing ratios are $\Delta[1\text{-}C_{10}H_9^+] : \Delta[1\text{-}C_{10}H_9] : \Delta[2\text{-}C_{10}H_9] : \Delta[C_{10}H_8] \cong -1.0 : 2.4 : 5.7 : -11.9$ according to Fig. 2(C) and the theoretically predicted IR intensities; the errors in measurements of integrated intensities are about 10% of the values. Upon irradiation with light at 365 nm for 2.5 h, $[1\text{-}C_{10}H_9^+] : [1\text{-}C_{10}H_9] : [2\text{-}C_{10}H_9] : [C_{10}H_8] = 1.0 : 12 : 1.1 : 59$ with $[C_{10}H_8] \cong 535$ ppm according to Fig. 2(D); the variations in mixing ratios are $\Delta[1\text{-}C_{10}H_9^+] : \Delta[1\text{-}C_{10}H_9] : \Delta[2\text{-}C_{10}H_9] : \Delta[C_{10}H_8] \cong -1.0 : 7.2 : -5.4 : -0.9$.

When the electron-bombarded matrix sample was irradiated with visible light (495–700 nm) from a filtered mercury lamp, the difference spectrum shows that the intensities of lines in group A ($1\text{-}C_{10}H_9$) increased, whereas those of group A^+ ($1\text{-}C_{10}H_9^+$) decreased, similar to the results after storage in darkness. Lines in group B ($2\text{-}C_{10}H_9$) also became more intense; irradiation of the matrix with visible light presumably releases only some electrons and H atoms originally trapped in the matrix but did not initiate substantial photolysis.[51] The variations in mixing ratios are $\Delta[1\text{-}C_{10}H_9^+] : \Delta[1\text{-}C_{10}H_9] : \Delta[2\text{-}C_{10}H_9] \cong -1.0 : 2.0 : 5.7$

Lines in an additional set, designated group B^+, with medium and weak ones at 1623.9, 1399.1, 1265.6, 1177.8, 1156.8, 935.3, 920.5, 799.2, and 767.7 cm^{-1} were observed only immediately upon irradiation at 365 nm for 10 min. We recorded the spectra consecutively with 100 scans (~3 min) in each step after irradiation of the electron-bombarded matrix sample with light at 365 nm. Traces (A) to (C) of Fig. 3 show difference spectra obtained on subtracting the spectrum recorded at the preceding step from that recorded at the present stage. In trace (A) the difference spectrum shows that upon irradiation of the matrix at 365 nm, the intensities of lines in group A^+ and B decreased (downward features), whereas, in addition to lines in group A that appeared as upward features, lines in group B^+ are clearly visible. In traces (B) and (C), the difference spectra indicate the variations after each data acquisition (without UV irradiation). The intensities of lines in group B^+ decreased continuously, whereas those of group A^+ increased. Lines of group B^+ became nearly completely eliminated after ~30 min.

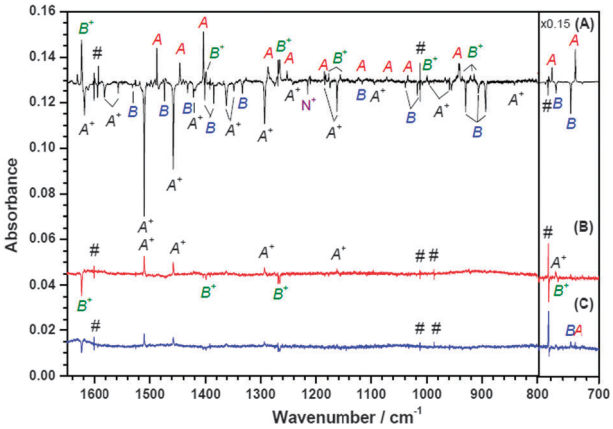

Fig. 3 Partial difference IR absorption spectra of the electron-bombarded $C_{10}H_8/p\text{-}H_2$ (1/1500) sample (A) recorded for 3 min immediately after irradiation at 365 nm for 10 min, (B) recorded during the next 8 min, (C) recorded during the following 9 min.

In experiments in another set, we placed a filter to eliminate IR light above 4000 cm^{-1} during acquisition of IR spectra, but lines in group B^+ also diminished during the course of a series of rapid data acquisitions. In a separate experiment, we irradiated the freshly deposited matrix (subjected to electron bombardment) at 365 nm and maintained it in darkness for 40 min before we began a series of rapid data acquisitions; we found that lines in group B^+ were absent. These experiments indicate that lines in group B^+ were converted to those in group A^+ spontaneously, even without IR irradiation. We assign these unstable features of group B^+ to $2\text{-}C_{10}H_9^+$, to be discussed in Section 5.3. A list of observed lines in group B^+ is given in Table 1.

After irradiation at 365 nm for 10 min, we estimated the concentrations of $1\text{-}C_{10}H_9^+$, $2\text{-}C_{10}H_9^+$, $1\text{-}C_{10}H_9$, $2\text{-}C_{10}H_9$, and naphthalene to be approximately 5, 4, 124, 8, and 540 ppm, and the variations in mixing ratios are approximately $\Delta[1\text{-}C_{10}H_9^+] : \Delta[2\text{-}C_{10}H_9^+] : \Delta[1\text{-}C_{10}H_9] : \Delta[2\text{-}C_{10}H_9] : \Delta[C_{10}H_8] = -1.0 : 0.3 : 4.2 : -3.4 : -1.0$ according to Fig. 3(A) and the theoretically predicted IR intensities; the errors are about 15% of the values. In Fig. 3(B) and (C), the variations in mixing ratios are $[1\text{-}C_{10}H_9^+] : [2\text{-}C_{10}H_9^+] = 1.0 : -1.0$; the errors are about 15% of the values.

5. Discussion

The intensities of lines in group A^+ decreased upon UV or visible irradiation, and also when the matrix was maintained in darkness for a prolonged period. Because electrons can diffuse slowly and recombine with cations in darkness, and because irradiation of the matrix with light at 365 nm or visible light is expected to release electrons trapped in the matrix and to neutralize cationic species,[51] lines in group A^+ are clearly associated with an ionic species. In contrast, because the intensities of lines in group A increased upon 365 nm or visible

irradiation and also when the matrix was maintained in darkness for 19 h, they are associated with a neutral species. The intensities of lines in group B increased when the matrix was maintained in darkness, but decreased upon irradiation at 365 nm. The carrier of these lines might be a neutral species that is subject to photodestruction at 365 nm. Lines in group B^+ were only observed immediately after photolysis at 365 nm; hence they are associated with an unstable species. We assign the carrier of each group as follows.

5.1 Assignment of lines in group A^+ to 1-$C_{10}H_9^+$

As discussed above, lines in group A^+ are associated with an ionic species. In our experiments we expect to produce one or more of the isomers of $C_{10}H_9^+$ upon electron bombardment of a mixture of *p*-H_2 and naphthalene. The spectrum of 1-$C_{10}H_9^+$ recorded with IRMPD[22] and that of 1-$C_{10}H_9^+$-Ar recorded with IRPD[24] are reproduced in traces (A) and (B) of Fig. 4, respectively, for comparison with observed features in group A^+ shown in Fig. 4(C). Lines in group A^+ are readily assigned to absorption of 1-$C_{10}H_9^+$ on comparison with the IRPD spectral features of gaseous 1-$C_{10}H_9^+$-Ar reported by Ricks *et al.*[24] The relative intensities and wavenumbers of major lines in Fig. 4(B) and (C) are mutually consistent except that the intensities of CH-stretching modes of $C_{10}H_9^+$-Ar reported by IRPD are much more intense. The discrepancy might be due partly to the increased laser energy and partly to the greater efficiency in dissociation of Ar-tagged species at greater frequencies. These features also agree satisfactorily with a stick spectrum shown in Fig. 4(D) that was simulated according to anharmonic vibrational wavenumbers and IR intensities computed with the B3PW91/6-311++G(2d,2p) method; the predicted harmonic and anharmonic vibrational wavenumbers are available in ESI† (Table S4). An intense line predicted near 772 cm^{-1} was overlapped with the intense absorption of 2-$C_{10}H_9$ at 771.4 cm^{-1}, designated as "?", but this band could be clearly identified at 772.0 cm^{-1} in Fig. 3(B).

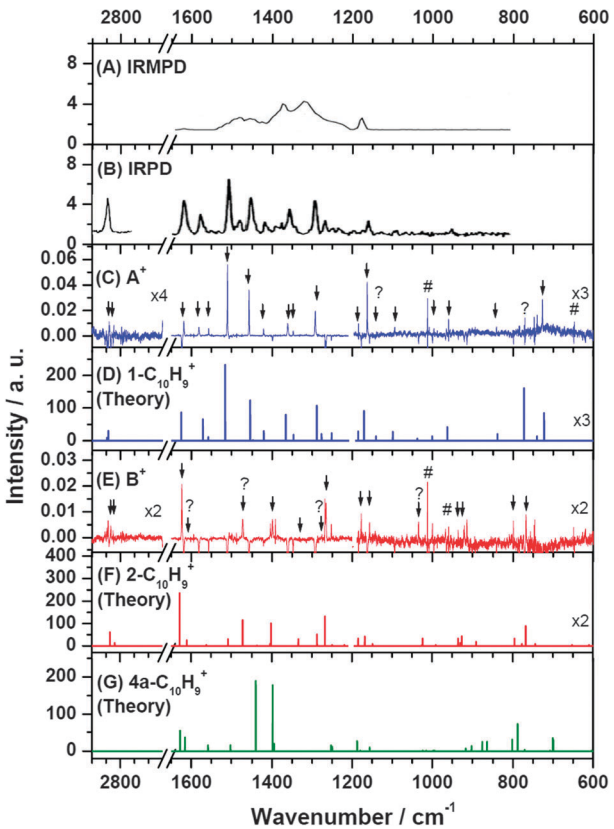

Fig. 4 Comparison of experimental IR absorption spectra of isomers of $C_{10}H_9^+$ with theoretical predictions. (A) Spectrum of $C_{10}H_9^+$ recorded with the IRMPD method (ref. 22), (B) spectrum of $C_{10}H_9$-Ar^+ recorded with the IRPD method (ref. 24), (C) spectrum of group A^+ recorded in this work derived from inverse Fig. 2(D) in which only positive lines are shown, (D) stick spectrum of 1-$C_{10}H_9^+$ simulated according to anharmonic vibrational wavenumbers and IR intensities calculated with the B3PW91/6-311++G(2d,2p) method, (E) spectrum of group B^+ recorded in this work, (F) stick spectrum of 2-$C_{10}H_9^+$, and (G) stick spectrum of 4a-$C_{10}H_9^+$ simulated similarly as in (D).

Table 1 shows a comparison of the observed wavenumbers of 1-$C_{10}H_9^+$-Ar, observed wavenumbers and relative IR intensities of 1-$C_{10}H_9^+$, and those predicted quantum-chemically for 1-$C_{10}H_9^+$. Our observed lines deviate from the predicted anharmonic vibrational wavenumbers by less than 10 cm^{-1} (0.8%) and almost all features in the spectral region of our detection with IR intensity greater than 7 km mol^{-1} were observed. Intense lines predicted near 1515 and 1458 cm^{-1} and observed at 1510.0 and 1457.9 cm^{-1} are due to ring-deformation modes, whereas those predicted near 2848, 2843, and 1286 cm^{-1} and observed at 2844.7, 2839.1, and 1292.4 cm^{-1} are characteristic of the symmetric stretching, antisymmetric stretching, and scissoring modes, respectively, of the CH_2 moiety. Taking into account all available information, the features of group A^+ are readily assigned to 1-$C_{10}H_9^+$. As illustrated in Fig. 4(B) and (C), our spectrum has much narrower lines than those reported for 1-$C_{10}H_9^+$-Ar using IRPD, so that lines from 2-$C_{10}H_9^+$ are readily distinguishable, to be discussed in Section 5.3.

5.2 Assignments of lines in groups A and B to 1-$C_{10}H_9$ and 2-$C_{10}H_9$

We reproduce lines in groups A and B in Fig. 5(A) and (C), respectively. As discussed above, lines in group A are associated with a neutral species and those in group B might be associated with a neutral species that is subject to photodestruction at 365 nm. Because the intensities of these lines in group A increase when those of 1-$C_{10}H_9^+$ decrease, they are likely associated with $C_{10}H_9$. To our knowledge, no IR spectrum of isolated $C_{10}H_9$ has been reported.

We performed quantum-chemical calculations at the B3PW91/6-311++G(2d,2p) level and located three stable isomers of $C_{10}H_9$, as shown in ESI† (Tables S1–S3 for the geometric parameters of these species and Fig. S3 for the potential energy surfaces of isomerization). The most stable isomer is 1-$C_{10}H_9$, of which the energy is 20.0 kJ mol^{-1} less than that of 2-$C_{10}H_9$. The isomer 4a-$C_{10}H_9$ is nonplanar, because it has an H atom attached to the carbon on the two fused rings; its energy is 103.3 kJ mol^{-1} greater than that of 1-$C_{10}H_9$. The anharmonic vibrational wavenumbers and IR intensities of these three

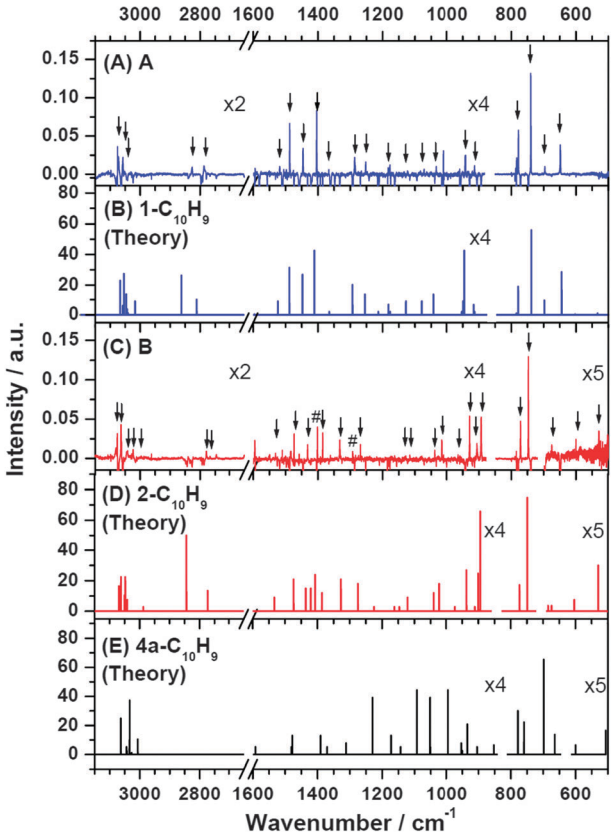

Fig. 5 Comparison of experimental IR absorption spectra of isomers of $C_{10}H_9$ with theoretical predictions; (A) spectrum of group A reproduced from Fig. 2(D), (B) stick spectrum of 1-$C_{10}H_9$ simulated according to anharmonic vibrational wavenumbers and IR intensities calculated with the B3PW91/6-311++G(2d,2p) method, (C) spectrum of group B recorded in this work, (D) stick spectrum of 2-$C_{10}H_9$, and (E) stick spectrum of 4a-$C_{10}H_9$ simulated similarly as in (B).

isomers have been predicted and listed in Table 2 for 1-$C_{10}H_9$ and 2-$C_{10}H_9$ and in Table S6 (ESI†) for 4a-$C_{10}H_9$. Comparison of harmonic and anharmonic vibrational wavenumbers is included in Tables S4–S6 (ESI†) for these three species and their cations. Stick spectra of 1-$C_{10}H_9$, 2-$C_{10}H_9$, and 4a-$C_{10}H_9$ simulated according to predicted anharmonic vibrational wavenumbers and IR intensities are shown in Fig. 5(B), (D), and (E), respectively.

Observed intense lines at 778.1, 739.8, and 648.5 cm^{-1}, and other weaker lines in group A, shown in Fig. 5(A), agree satisfactorily with those predicted for 1-$C_{10}H_9$, shown in Fig. 5(B), in terms of positions and relative intensities. The characteristic symmetric and antisymmetric CH_2 stretching modes predicted near 2865 and 2817 cm^{-1} were observed at 2843.5 (ν_8) and 2787.1 (ν_{35}) cm^{-1}. The CH_2 scissoring mode was predicted near 1411 cm^{-1} and observed at 1403.9 cm^{-1}. Two additional intense lines predicted near 3074 and 3061 cm^{-1} for CH-stretching modes were observed at 3073.0 and 3057.4 cm^{-1}. The observed wavenumbers and relative integrated intensities in group A are compared with the predicted anharmonic vibrational wavenumbers and IR intensities of 1-$C_{10}H_9$ in Table 2. The average deviation between observed and predicted wavenumbers is 4.8 cm^{-1}. The largest deviation in wavenumbers is 29.9 cm^{-1} (1.1%) for ν_{35}, still within expected computational errors. We thus assigned the carrier of lines in groups A to 1-$C_{10}H_9$.

Similarly, the two most intense lines observed at 771.4 and 747.1 cm^{-1} in group B agree satisfactorily with two lines predicted near 773 and 749 cm^{-1} for 2-$C_{10}H_9$. All observed lines in group B, shown in Fig. 5(C), agree satisfactorily with the spectrum predicted for 2-$C_{10}H_9$, shown in Fig. 5(D), in terms of line positions and relative intensities. The characteristic symmetric and antisymmetric CH_2 stretching modes of 2-$C_{10}H_9$ predicted near 2844 and 2773 cm^{-1} were observed at 2795.8 (ν_8) and 2779.2 (ν_{35}) cm^{-1}. Two additional intense lines of CH-stretching modes predicted near 3062 and 3048 cm^{-1} were observed at 3063.9 and 3045.3 cm^{-1}. The CH_2 scissoring mode was predicted near 1407 cm^{-1} and observed at 1401.3 cm^{-1}. The observed wavenumbers and relative integrated intensities in group B are compared with the predicted anharmonic vibrational wavenumbers and IR intensities of 2-$C_{10}H_9$ in Table 2. The average deviation between observed and predicted wavenumbers is 7.0 cm^{-1}; the largest deviation in wavenumbers is 48 cm^{-1} (1.7%) for ν_8, within expected computational errors. We thus assigned the carrier of lines in group B to 2-$C_{10}H_9$.

5.3 Assignments of lines in group B^+ to 2-$C_{10}H_9^+$

As described in the preceding section, the decay of the intensities of lines in group B^+ was observed through a series of IR spectra recorded at ~3 min intervals after irradiation of the matrix at 365 nm (Fig. 3). The observed pattern of lines in group B^+ is similar to that of lines in group A^+ (1-$C_{10}H_9^+$) with intense lines distributed in the 1200–1650 cm^{-1} region, but is unlike those of lines in groups A (1-$C_{10}H_9$) and B (2-$C_{10}H_9$) that have intense lines in the 600–800 cm^{-1} region. Hence, the most likely carrier for lines in group B^+ is either 2-$C_{10}H_9^+$ or 4a-$C_{10}H_9^+$.

We performed quantum-chemical calculations at the B3PW91/6-311++G(2d, 2p) level and located, in addition to 1-$C_{10}H_9^+$, two other isomers of $C_{10}H_9^+$. Isomer 2-$C_{10}H_9^+$ has energy 12.1 kJ mol^{-1} greater than that of 1-$C_{10}H_9^+$, whereas the energy of isomer 4a-$C_{10}H_9^+$ is 78.0 kJ mol^{-1} greater than that of 1-$C_{10}H_9^+$. These values are similar to the previous report of 12 and 80 kJ mol^{-1} for 2-$C_{10}H_9^+$ and 4a-$C_{10}H_9^+$, respectively.[22] The anharmonic vibrational wavenumbers and IR intensities of 2-$C_{10}H_9^+$ and 4a-$C_{10}H_9^+$, predicted with the B3PW91/6-311++G(2d,2p) method, are listed in Table 1 for 1-$C_{10}H_9^+$ and 2-$C_{10}H_9^+$ and in Table S6 (ESI†) for 4a-$C_{10}H_9^+$. We reproduced the spectrum of lines in group B^+ in Fig. 4(E) by stripping lines of A^+, A, and B from trace (A) of Fig. 3 so that some lines of B^+ overlapped with intense lines of A^+, A, and B might be extracted and shown. Lines of group B^+ at 1472.0, 1177.8, and 1034.3 cm^{-1} were extracted from the overlapped bands and shown in Fig. 4(E) with "?" marks indicating that the intensities of these bands remain tentative. Because of the rapid decay of these lines, the ratio of signal to noise is less satisfactory than that of groups A^+, A, and B. We plot the stick spectra of 2-$C_{10}H_9^+$ and 4a-$C_{10}H_9^+$, simulated according to predicted anharmonic vibrational wavenumbers and IR intensities, in Fig. 4(F) and (G), respectively.

The spectral pattern of lines in group B^+, shown in Fig. 4(E), agrees satisfactorily with the spectrum predicted for 2-$C_{10}H_9^+$, shown in Fig. 4(F), but not with that of 4a-$C_{10}H_9^+$, shown in Fig. 4(G), in terms of line positions and relative intensities. The two most intense lines of 2-$C_{10}H_9^+$ observed at 1623.9 cm^{-1} (ν_9, ring deformation) and at 1265.6 cm^{-1} (ν_{19}, in-plane CH bend) are consistent with the predicted values of 1627 and 1268 cm^{-1}, respectively. Two additional intense lines of 2-$C_{10}H_9^+$ were predicted to be near 1471 and 1507 cm^{-1}, but observed lines at 1472.0 and 1505.4 cm^{-1} have smaller intensities. The discrepancy might be due partly to errors in calculations of IR intensity and partly to possible interference from the nearby intense lines of 1-$C_{10}H_9^+$ (1510.0 cm^{-1}) and 2-$C_{10}H_9$ (1473.4 cm^{-1}). Lines predicted near 2835 and 2819 cm^{-1}, observed at 2829.4 and 2819.3 cm^{-1}, are characteristic of the symmetric and antisymmetric stretching modes, respectively, of the CH_2 moiety. The line predicted near 1289 cm^{-1} for the CH_2 scissor was unobserved, likely overlapped with that of 1-$C_{10}H_9^+$. The observed wavenumbers and relative integrated intensities in group B^+ are compared with the predicted anharmonic vibrational wavenumbers and IR intensities of 2-$C_{10}H_9^+$ in Table 1. The average deviation between observed and predicted wavenumbers is 5.5 cm^{-1}. The largest deviation in wavenumbers is 11.3 cm^{-1} (1.1%) for ν_{25}, also within expected computational errors. We thus assigned the carrier of lines in group B^+ to 2-$C_{10}H_9^+$.

5.4 Mechanism of formation and comparison with preceding experimental results

As illustrated in Fig. 4(A) and (C), although the widths of lines in the IRPD spectrum of 1-$C_{10}H_9^+$-Ar[24] are much smaller than those of the IRMPD spectrum for 1-$C_{10}H_9^+$,[22] the spectral resolution remains insufficient to resolve contributions from 2-$C_{10}H_9^+$. The line widths of 1-$C_{10}H_9^+$ observed in solid p-H_2 are much smaller than those reported for 1-$C_{10}H_9^+$-Ar in a jet, and the spectral region was extended from 950 cm^{-1} to 600 cm^{-1}. With the improved ratio of signal to noise, our experiments can clearly distinguish the two isomers of $C_{10}H_9^+$. By comparison with our spectra, lines at 1480, 1391, and 1252 cm^{-1}, and partially at 1617 cm^{-1} observed in the IRPD experiment of Ar-tagged $C_{10}H_9^+$ might be due to 2-$C_{10}H_9^+$-Ar. Furthermore, because the IRPD spectrum is an action spectrum that has greater efficiencies of dissociation of Ar-tagged molecules at large wavenumbers, the reported spectrum tends to show intensity in the C–H stretching region much greater than that predicted. Our observed line intensities in this region agree better with predictions.

1-$C_{10}H_9^+$, 1-$C_{10}H_9$, and 2-$C_{10}H_9$ were observed upon electron-bombardment of a matrix sample of $C_{10}H_8$–p-H_2 during deposition. In contrast, no spectral feature due to 2-$C_{10}H_9^+$ was observed upon deposition, but, because of the instability of 2-$C_{10}H_9^+$, the possibility of its formation during deposition cannot be excluded. After the matrix was maintained in darkness for several hours, the intensities of lines of 1-$C_{10}H_9^+$ decreased whereas those of 1-$C_{10}H_9$ and 2-$C_{10}H_9$ increased, indicating that neutralization of 1-$C_{10}H_9^+$ yields both 1-$C_{10}H_9$ and 2-$C_{10}H_9$. The enthalpy of neutralization for 1-$C_{10}H_9^+$ is 624 kJ mol^{-1}.[52] The barrier for isomerization from 1-$C_{10}H_9$ to 2-$C_{10}H_9$ is predicted to be about 171 kJ mol^{-1}. It is possible that the neutralization also induces isomerization between 1-$C_{10}H_9$ and 2-$C_{10}H_9$ in solid p-H_2. The observed variation in the mixing ratio $\Delta[1\text{-}C_{10}H_9^+] : \Delta[1\text{-}C_{10}H_9] : \Delta[2\text{-}C_{10}H_9] \cong -1.0 : 2.4 : 5.7$ indicates that the formation of 2-$C_{10}H_9$ is more favored than 1-$C_{10}H_9$. Retention of the isomeric structure was reported during neutralization of 1-$C_{10}H_9^+$ and 2-$C_{10}H_9^+$ in a Ne matrix.[21] Apparently additional processes to yield 1-$C_{10}H_9$ and 2-$C_{10}H_9$ exist. We further examined the decrease of naphthalene as a function of time when the matrix was maintained in the dark at 3.3 K and found that the decrease in the mixing ratio of naphthalene correlated well with the sum of the increase in mixing ratios of 1-$C_{10}H_9$ and 2-$C_{10}H_9$. The reaction of the originally trapped H atoms with $C_{10}H_8$ might account for the main source of formation of these neutral species.[53] The exothermicity of reactions H + $C_{10}H_8$ → 1-$C_{10}H_9$ and 2-$C_{10}H_9$ was predicted to be 109 and 89 kJ mol^{-1}, respectively.[52]

Although irradiation of the matrix with UV light showed an efficiency of neutralization much more enhanced than that with visible light or on maintaining the matrix in darkness for a prolonged period, it might also induce photoisomerization or photodissociation, as indicated by the decreased intensity of 2-$C_{10}H_9$. The smallest C–H bond energies of 1-$C_{10}H_9$ and 2-$C_{10}H_9$ were determined to be 121 and 104 kJ mol^{-1}, respectively;[31] irradiation with the 365-nm photon (328 kJ mol^{-1}) might hence dissociate the C–H bond of either radical. The observed variation in mixing ratio $\Delta[1\text{-}C_{10}H_9^+] : \Delta[1\text{-}C_{10}H_9] : \Delta[2\text{-}C_{10}H_9] \cong -1 : 7.2 : -5.4$ indicates that the major process upon irradiation at 365 nm is the conversion of 2-$C_{10}H_9$ to 1-$C_{10}H_9$ and a minor process is the destruction of 1-$C_{10}H_9^+$ due to neutralization or other processes. In a separate experiment, we found that irradiation at 254 nm converted 1-$C_{10}H_9$ into 2-$C_{10}H_9$.

The observation of 2-$C_{10}H_9^+$ at the expense of 1-$C_{10}H_9^+$ upon irradiation of the matrix at 365 nm indicates that some 1-$C_{10}H_9^+$ is photoconverted to 2-$C_{10}H_9^+$ at this wavelength. This observation is consistent with a report that irradiation in the range 350–390 nm induces tautomerization of 1-$C_{10}H_9^+$ → 2-$C_{10}H_9^+$; the wavelength region corresponds to the $S_2 \leftarrow S_0$ absorption of 1-$C_{10}H_9^+$.[21]

The rapid decay of 2-$C_{10}H_9^+$ in darkness indicates that 2-$C_{10}H_9^+$ is unstable. From Fig 3(B) and (C), 2-$C_{10}H_9^+$ is clearly converted to 1-$C_{10}H_9^+$. The barrier for isomerization of 2-$C_{10}H_9^+$ → 1-$C_{10}H_9^+$ is calculated to be ~32 kJ mol^{-1}, whereas that of the reverse reaction is 47 kJ mol^{-1}.[21] At 3.2 K in darkness, the only possible path would be quantum tunneling of the labile proton. This instability of 2-$C_{10}H_9^+$ was reported also in solid Ne.[21]

6. Conclusion

Electron bombardment during deposition of a mixture of $C_{10}H_8$ and p-H_2 at 3.2 K was employed to generate 1-$C_{10}H_9^+$, 1-$C_{10}H_9$, and 2-$C_{10}H_9$. The intensities of lines due to the neutral species 1-$C_{10}H_9$ and 2-$C_{10}H_9$ increased whereas those of 1-$C_{10}H_9^+$

decreased when the matrix was maintained in darkness for a long period or irradiated with visible light. Irradiation of the matrix with UV light at 365 nm diminished the lines of 1-$C_{10}H_9^+$ and 2-$C_{10}H_9$, whereas the intensities of those of 1-$C_{10}H_9$ increased, indicating significant conversion of 1-$C_{10}H_9$ to 2-$C_{10}H_9$ at this wavelength. Lines of 2-$C_{10}H_9^+$ were observed only within 30 min after irradiation of the matrix at 365 nm; it converts to 1-$C_{10}H_9^+$ likely through quantum tunneling. These lines were identified according to their behavior at successive stages of experiments and assigned according to the expected chemistry, comparison with previous reports (for 1-$C_{10}H_9^+$) and anharmonic vibrational wavenumbers and IR intensities predicted for various isomers of $C_{10}H_9^+$ and $C_{10}H_9$. IR spectra of 2-$C_{10}H_9^+$, 1-$C_{10}H_9$, and 2-$C_{10}H_9$ are new.

Our spectra exhibit a much improved ratio of signal to noise with spectral lines much narrower than those obtained from other techniques; most close-lying lines of isomers 1-$C_{10}H_9^+$/2-$C_{10}H_9^+$ and 1-$C_{10}H_9$/2-$C_{10}H_9$ were clearly resolved and identified. Except a few overlapped lines, nearly all lines predicted with IR intensities greater than 7 km mol^{-1} have been observed. This method is also clean, with production of mainly 1-$C_{10}H_9^+$, 1-$C_{10}H_9$, and 2-$C_{10}H_9$, without much interference from other byproducts, especially those from fragmentation. Although absorptions of 1-$C_{10}H_9^+$, 2-$C_{10}H_9^+$, 1-$C_{10}H_9$, and 2-$C_{10}H_9$ do not match features in the UIR emission, and the intensity ratio measured in this work might be different from emission,[54,55] this method proves to be suitable for the investigation of IR spectra of higher protonated PAH.

Acknowledgements

The National Science Council of Taiwan supported this work under contract NSC100-2745-M-009-001-ASP. YJW acknowledges support from Beamline 14A at the National Synchrotron Radiation Research Center (NSRRC) of Taiwan. The National Center for High-Performance Computing provided computer time. We thank John Maier for providing a preprint.

Notes and references

1 O. Dopfer, *PAHs and the Universe*, ed. C. Joblin and A. G. G. M. Tielens, EAS Publication Series, 2011, vol. 46, p. 103.
2 A. G. G. M. Tielens, *Annu. Rev. Astron. Astrophys.*, 2008, **46**, 289.
3 A. G. G. M. Tielens, *The Physics and Chemistry of the Interstellar Medium*, Cambridge University Press, Cambridge, UK, 2005.
4 D. M. Hudgins and L. J. Allamandola, *Astrophys. J.*, 1999, **513**, L69.
5 B. T. Draine and A. Li, *Astrophys. J.*, 2007, **657**, 810.
6 S. Kwok and Y. Zhang, *Nature*, 2011, **479**, 80.
7 H. A. Galué and J. Oomens, *Astrophys. J.*, 2012, **746**, 83.
8 D. M. Hudgins, C. W. Bauschlicher, Jr. and L. J. Allamandola, *Spectrochim. Acta, Part A*, 2001, **57**, 907.
9 A. I. S. Holm, H. A. B. Johansson, H. Cederquist and H. Zettergren, *J. Chem. Phys.*, 2011, **134**, 044301.
10 L. J. Allamandola, D. M. Hudgins and S. A. Sandford, *Astrophys. J.*, 1999, **511**, L115.
11 T. P. Snow, V. Le Page, Y. Keheyan and V. M. Bierbaum, *Nature*, 1998, **391**, 259.
12 G. A. Olah, *Acc. Chem. Res.*, 1971, **4**, 240.
13 A. B. Fialkov, J. Dennebaum and K. H. Homsnn, *Combust. Flame*, 2001, **125**, 763.
14 A. Kiendler and F. Arnold, *Atmos. Environ.*, 2002, **I36I**, 2979.
15 A. J. Coates, F. J. Crary, G. R. Lewis, D. T. Young, J. H. Waite and E. C. Sittler, *Geophys. Res. Lett.*, 2007, **34**, L22103.
16 J. H. Waite, D. T. Young, T. E. Cravens, A. J. Coates, F. J. Crary, B. Magee and J. Westlake, *Science*, 2007, **316**, 870.
17 D. Kovacek, Z. B. Maksic and I. Novak, *J. Phys. Chem. A*, 1998, **102**, 329.
18 G. A. Olah, G. D. Mateescu and Y. K. Mo, *J. Am. Chem. Soc.*, 1973, **95**, 1865.
19 I. Alata, R. Omidyan, M. Broquier, C. Dedonder, O. Dopfer and C. Jouvet, *Phys. Chem. Chem. Phys.*, 2010, **12**, 14456.
20 I. Alata, C. Dedonder, M. Broquier, E. Marceca and C. Jouvet, *J. Am. Chem. Soc.*, 2010, **132**, 17483.
21 I. Garkusha, A. Nagy, J. Fulara, M. F. Rode, A. L. Sobolewski and J. P. Maier, *J. Phys. Chem. A* (in press).
22 U. J. Lorenz, N. Solcá, J. Lemaire, P. Maître and O. Dopfer, *Angew. Chem., Int. Ed.*, 2007, **46**, 6714.
23 H. Knorke, J. Langer, J. Oomens and O. Dopfer, *Astrophys. J. Lett.*, 2009, **706**, L66.
24 A. M. Ricks, G. E. Douberly and M. A. Duncan, *Astrophys. J.*, 2009, **702**, 301.
25 C. S. McEnally, L. D. Pfefferle, B. Atakan and K. Kohse-Hoinghaus, *Prog. Energy Combust. Sci.*, 2006, **32**, 247.
26 C. W. Jacobsen, H. K. Hong and S. J. Sheng, *J. Phys. Chem.*, 1978, **82**, 1537.
27 K. Nakagawa and N. Itoh, *Chem. Phys.*, 1976, **16**, 461.
28 V. A. Smironv, O. M. Andreev and M. V. Alfimov, *Chem. Phys. Lett.*, 1974, **28**, 84.
29 T. Nakayama and S. J. Sheng, *J. Phys. Chem.*, 1979, **83**, 2869.
30 I. D. Reid and E. Roduner, *Struct. Chem.*, 1991, **2**, 419.
31 J. A. Sebree, V. V. Kislov, A. M. Mebel and T. S. Zwier, *J. Phys. Chem. A*, 2010, **114**, 6255.
32 M. Bahou, Y.-J. Wu and Y.-P. Lee, *J. Chem. Phys.*, 2012, **136**, 154304.
33 V. I. Feldman, F. F. Sukhov, E. A. Logacheva, A. Y. Orlov, I. V. Tyulpina and D. A. Tyurin, *Chem. Phys. Lett.*, 2007, **437**, 207.
34 Y.-P. Lee, Y.-J. Wu, R. M. Lees, L.-H. Xu and J. T. Hougen, *Science*, 2006, **311**, 365.
35 M. Bahou and Y.-P. Lee, *J. Chem. Phys.*, 2010, **133**, 164316.
36 M. J. Frisch, *et al.*, *GAUSSIAN 09, Revision A.02*, Gaussian, Inc., Wallingford, CT, USA, 2009.
37 A. D. Becke, *J. Chem. Phys.*, 1993, **98**, 5648.
38 J. P. Perdew, K. Burke and Y. Wang, *Phys. Rev. B: Condens. Matter Mater. Phys.*, 1996, **54**, 16533.
39 D. M. Hudgins, S. A. Sandford and L. J. Allamandola, *J. Phys. Chem.*, 1994, **98**, 4243.
40 J. E. Roser and L. J. Allamandola, *Astrophys. J.*, 2010, **722**, 1932.

41 A. L. McClellan and G. C. Pimentel, *J. Chem. Phys.*, 1955, **23**, 245.
42 E. R. Lippincott and E. J. O'Reilly, Jr., *J. Chem. Phys.*, 1955, **23**, 238.
43 S. C. Wait and F. E. Shaffer, *J. Mol. Spectrosc.*, 1963, **10**, 78.
44 K. B. Hewett, M. Shen, C. L. Brummel and L. A. Philips, *J. Chem. Phys.*, 1994, **100**, 4077.
45 O. Pirali, M. Vervloet, G. Mulas, G. Malloci and C. Joblin, *Phys. Chem. Chem. Phys.*, 2009, **11**, 3443.
46 S. Albert, K. K. Albert, P. Lerch and M. Quack, *Faraday Discuss.*, 2011, **150**, 71.
47 M. C. R. Cockett, H. Ozeki, K. Okuyama and K. Kimura, *J. Chem. Phys.*, 1993, **98**, 7763.
48 J. Schiedt, W. J. Knott, K. Le Barbu, E. W. Schlag and R. Weinkauf, *J. Chem. Phys.*, 2000, **113**, 9470.
49 J. K. Song, S. Y. Han, I. H. Chu, J. H. Kim, S. K. Kim, S. A. Lyapustina, S. J. Xu, J. M. Nilles and K. H. Bowen, *J. Chem. Phys.*, 2002, **116**, 4477.
50 C. L. Dodson and J. F. Graham, *J. Phys. Chem.*, 1973, **77**, 2903.
51 L. B. Knight, Jr. and J. Steadman, *J. Am. Chem. Soc.*, 1984, **106**, 900.
52 J. A. Sebree, V. V. Kislov, A. M. Mebel and T. S. Zwier, *Faraday Discuss.*, 2010, **147**, 231.
53 M. Fushitani and T. Momose, *Low Temp. Phys.*, 2003, **29**, 740.
54 D. R. Wagner, H. S. Kim and R. J. Saykally, *Astrophys. J.*, 2000, **545**, 854.
55 S. Schlemmer, D. J. Cook, J. A. Harrison, N. Balucani, B. Wurfel, W. Chapman and R. J. Saykally, *Science*, 1994, **265**, 1686.